Design of Decoupled Fuzzy Controller to Enhance the Transient Performance For the Current Control of PMSG Based Wind Turbine

R.Vyshna
(P.G Student)(M.E P.E.D) ,
Narayanaguru College of Engineering,
Tamil Nadu,India,
vyshnakrishnan96@gmail.com.

R.Priyadarsini
Assistant Professor, B.E,M.E, Ph.D),
Narayanaguru College of Engineering,
Tamil Nadu,India,
priya_11darshini@yahoo.co.in

S.V Dishore
Assistant Professor, B.Tech,M.Tech,(Ph.D),
Narayanaguru College of Engineering,
Tamil Nadu,India,
dishore312@gmail.com.

***Abstract*—This paper presents a novel design process of decoupled PI current controller for permanent magnet synchronous generator (PMSG)-based wind turbines feeding a grid-tied inverter through back-to-back converter. Specifically, the design methodology consists of combining disturbance observer-based control (DOBC) with feedback linearization (FBL) technique to ensure nominal transient performance recovery under model uncertainty. By simplifying the DOBC under the feedback linearizing control, it is shown that the composite controller reduces to a decoupled PI current controller plus an additional term that has the main role of recovering the nominal transient performance of the feedback linearization, especially under step changes in the reference. Additionally, an anti-windup compensator arises naturally into the controller when considering the control input saturation to design the DOBC. This permits to remove the effect of the saturation blocks required to limit the control input. The proposed control scheme is implemented and validated through experimentation conducted on 22-pole, 5 kW PMSG. The results revealed that the proposed technique can successfully achieve nominal performance recovery under model uncertainty as well as improved transient performances under control saturation.**

***Index Terms*—Anti-windup scheme, disturbance observer, nominal performance recovery, permanent magnet synchronous generator (PMSG), PI controller, renewable energy, wind energy conversion system.**

I. Introduction

In grid-connected applications, back-to-back converter is commonly used to control the power exchange between the host grid and the PMSG-based wind energy conversion system (WECS) as shown in Fig. 1. This type of converter consists of a Machine Side Converter (MSC) and a Grid Side Converter (GSC) that are interconnected through a DC-link capacitor [1]. The role of each converter depends on the operating conditions such as maximum power point tracking (MPPT), low-voltage Specifically, under the assumption that the DC-link voltage is well regulated, the main objective of this work is to design a PI current controller for the PMSG-based WECS that is able to achieve a good transient performance, and not just asymptotic regulation under model uncertainty.

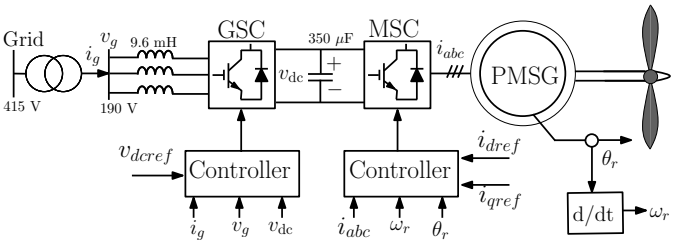

Fig. 1. Configuration of a direct-drive PMSG-based WECS connected to the host grid.

ride through (LVRT), power oscillation damping [2], etc. In this work, the GSC is employed to regulate the DC-link voltage and the reactive power fed to the grid to comply with the grid codes. The control design for the GSC is not discussed here, and it is considered beyond the scope of this work. Relying on the assumption that the DC-link voltage is tightly regulated, MSC controls the PMSG output power/torque by means of stator current regulation. To do so, the reference for the q-axis current i_{qref} is selected to correspond to the torque command by exploring the direct relation between the developed torque, the direct d-axis component i_d, and the quadrature q-axis component i_q. The reference for the d-axis current is set to be equal to zero as in [3]. The q-axis current reference can also be generated through the use of an outer loop to either control the rotor speed under MPPT operation [4] or regulate the DC-link voltage under abnormal conditions such as grid voltage fault [5]. Designing a controller for the PMSG-based WECS under abnormal conditions is an important area of research itself. This explains why this work is only dedicated to the case of normal conditions, ie., the three-phase grid voltage is assumed to be balanced.

There are various control techniques that have been applied to PMSG to achieve good transient and steady-state performances. In [6], a linear parameter-varying (LPV) technique has been adopted to achieve a robust control of the PMSG-based WECS in the presence of model uncertainty.

LPV control scheme is inspired from H_∞ optimal control procedure; therefore, its design requires the use of advanced optimization techniques. The need for solving an optimization problem raises concerns about the complexity of the control design. An attempt to design a simple and robust controller for the PMSG-based WECS was through sliding mode controller (SMC) [7], [8]. The SMC technique provides an opportunity for tighter guarantees on robustness against parameter variation, but it suffers from chattering problem. Direct torque control (DTC) [9] has been introduced to improve the transient performance of the electric machines. DTC technique is attractive because it permits to obtain a good dynamic performance, and it is simple to implement. Although DTC approach has gained a great attention in both industry and academia, it suffers from irregular torque and flux ripples because of the variability of the switching frequency. An attempt to reduce the torque ripples in DTC scheme for PMSG-based WECS was through the use of different topologies of the MSC such as Vienna-rectifier [10]. Available methods for replacing DTC with reduced torque ripples are mainly inspired from model predictive control (MPC) approach [11]–[13]. The key idea is to evaluate a cost function using all possible voltage vectors to select the appropriate one based on an optimality criterion [14]. Such a technique, known as finite control set-model predictive control (FCS-MPC), is starting to receive attention in both industry and literature. The main drawback of FCS-MPC is that exact model parameters are required to accurately predict the behavior of the system over the prediction horizon, raising concerns about the robustness of this method against model parameter variation. To allow for uncertain parameters, integral action with a large time constant can be combined with this type of controller to eliminate the steady-state error under limited prediction accuracy [15]. Assuming directly an integral action in the controller may degrade the transient performance of the closed-loop system.

Field oriented control (FOC), known also as vector control (VC), is widely used in industry to control electric machines because it provides a less-complex controller and a good transient performance. In VC technique, a decoupled PI controller is usually adopted to control the d-axis and q-axis currents with the compensation of the effective back-EMF. In [16], a decoupled PI current controller was used to control the PMSG-based WECS, where a saturation mechanism was incorporated into the controller to limit the amplitude of the voltage reference. The introduction of the saturation mechanism prevents the MSC to enter into the nonlinear modulation mode. Nonetheless, the integral control during saturation may degrade the transient performances because of the integrator buildup. This performance loss can be reduced by adding an anti-windup compensator to the controller [17]. As in [17], a simple way to determine the parameters of the PI current controller for PMSG is the use of internal model principle. The latter considers the nominal parameters of the machine to tune the coefficients of the PI controller based on the specifications of the closed-loop transient response. The price, however, is that the nominal transient response cannot be retained under model uncertainty because of the direct relation between the control design and the machine parameters. The PI current controller is usually designed using the *dq* coordinates. An alternative way to implement PI current controller in the stationary reference frame is the use of proportional resonant (PR) controller [18]. The main idea of the PR controller is to set its resonance frequency to be equal to the fundamental frequency of the stator voltage, which is proportional to the rotor speed. The need for exact information about the fundamental frequency made the PR controller to be highly sensitive to the change of the rotor speed.

The majority of reported research works mostly focus on the regulation problem without considering the nominal performance recovery when dealing with model uncertainty. To retain the transient performance of the nominal closed-loop system, it is typical to combine a baseline controller with either integral sliding mode control (ISMC) [19], [20] or a disturbance observer-based control (DOBC) [21]. Both ISMC and DOBC have been proven to be effective in dealing with nominal performance recovery under model uncertainty. However, ISMC cannot be directly applied to control the switching power converter without continuous approximation of the control input to reduce the chattering effect. The method proposed in this paper is based on combining a DOBC with a feedback linearization technique. The proposed DOBC is basically a reduced-order high-gain observer [22]. Therefore, as pointed out in [21], for sufficiently fast observer, the composite controller can recover the nominal transient performance specified under feedback linearization method despite the presence of model uncertainty. Feedback linearization technique has been already used in the control of the PMSG-based WECS [23], [24], but none of the existing feedback controllers considers the nominal transient performance property. The main contribution of this work is in proving that the composite controller, for PMSG-based wind turbine, can be reduced to a decoupled PI current controller that includes both the reference jump and an anti-windup compensator. Therefore, the proposed approach is more suitable for real-time implementation, as it removes the need for integrating the system model required to implement DOBC. Compared with the existing decoupled PI current controller, the introduction of the reference jump greatly improves the transient performance of the closed-loop system in spite of model uncertainty. Another salient feature of the proposed PI current controller is that an anti-windup scheme arises systematically into the controller to cope with control input limitation, particularly when the modulating signal saturates because of the limited DC-link voltage. The main contributions of this paper can be summarized as follows:

- Proposing a novel control design of a PI current controller for PMSG-based wind energy conversion system, which can be considered as the modification of the existing PI current controller to achieve good transient performances, and not just asymptotic stabilization.
- Under unsaturated control, the proposed PI current controller is able to retain the nominal transient response achieved under feedback controller even in the presence of model uncertainty and external disturbance.
- During the control saturation, the proposed PI current

controller has a significant ability to cope with the windup phenomenon, leading to a good transient performance.

II. Design of the Baseline Controller

A. Modeling of PMSG

By neglecting the iron losses in the machine, the electric dynamics equations of the PMSG can be expressed in the rotor reference frame as follows

$$\begin{cases} \dot{\boldsymbol{x}} = \boldsymbol{f}(\boldsymbol{x}) + B\boldsymbol{u} + B\boldsymbol{b} \\ \boldsymbol{y} = \boldsymbol{h}(\boldsymbol{x}) \end{cases} \tag{1}$$

where

$$\boldsymbol{x} = \begin{bmatrix} i_d & i_q \end{bmatrix}^{\intercal}; \quad \boldsymbol{u} = \begin{bmatrix} u_d & u_q \end{bmatrix}^{\intercal} \tag{2}$$

and

$$\boldsymbol{b} = \begin{bmatrix} b_d & b_q \end{bmatrix}^{\intercal} \tag{3}$$

The disturbance vector $\boldsymbol{b}$ represents model uncertainty, PWM offset, and external disturbances, and it is assumed to be bounded. i_d and i_q are the d-axis and q-axis components of the armature current, respectively. u_d and u_q represent the d-axis and q-axis components of the armature voltage. $\boldsymbol{y}$ represents the system output to be controlled. The control matrix B is a 2×2 constant matrix, and it is given by

$$B = diag\{\frac{1}{L_d}, \frac{1}{L_q}\} \tag{4}$$

where L_d and L_q are the d-axis and q-axis inductances. The vector functions $\boldsymbol{f}(\boldsymbol{x})$ is defined as follows

$$\boldsymbol{f}(\boldsymbol{x}) = \begin{bmatrix} f_d(\boldsymbol{x}) \\ f_q(\boldsymbol{x}) \end{bmatrix} = \begin{bmatrix} -\frac{R}{L_d} i_d + \frac{L_q}{L_d} p\omega_r i_q \\ -\frac{R}{L_q} i_q - \frac{L_d}{L_q} p\omega_r i_d - \frac{\phi_v p\omega_r}{L_q} \end{bmatrix} \tag{5}$$

where ϕ_v, p, and R represent the permanent magnet flux, the number of pole pairs, and the per-phase armature resistance, respectively. ω_r is the rotor speed of the PMSG. The control objective is to regulate the torque T_g produced by the PMSG, which has the form

$$T_g = \frac{3}{2} p\left(\phi_v + (L_d - L_q) i_d\right) i_q \tag{6}$$

By forcing the d-axis current to be equal to zero, the q-axis current can be regulated to correspond to the desired torque. That is

$$\boldsymbol{y} = \boldsymbol{h}(\boldsymbol{x}) = \boldsymbol{x} = \begin{bmatrix} i_d & i_q \end{bmatrix}^{\intercal} \tag{7}$$

For a given rotor speed ω_r, the extracted power is given by $P_g = T_g\omega_r = 1.5p\phi_v\omega_r i_q$. Thus, with $\omega_r > 0$, selecting $i_q < 0$ makes the machine generate the power as $P_g < 0$. However, with $\omega_r < 0$, the q-axis current reference should be positive to make the machine operate as a generator.

B. Baseline Controller Design

As all states are available for measurement, the control objective can be achieved using a feedback linearization (FBL) technique. Toward this end, it is required to compute the relative degrees ρ_d and ρ_q that correspond to the outputs i_d and i_q, respectively. From (1)–(7), it follows that the relative degree ρ_d is equal to one, as the control input u_d appears in $\dot{i}_d$ [25]. In the same manner, it can be shown that $\rho_q = 1$. The relative degree ρ of the system is defined as $\rho = \rho_d + \rho_q = 2$. Since the relative degree ρ is equal to the order of the system, the closed-loop system under feedback linearizing control does not include zero dynamics. Following [25], a feedback linearizing control is then given by

$$\boldsymbol{u_0} = B^{-1} \begin{bmatrix} K_d e_d + \dot{i}_{dref} - f_d(\boldsymbol{x}) \\ K_q e_q + \dot{i}_{qref} - f_q(\boldsymbol{x}) \end{bmatrix} - \begin{bmatrix} b_d \\ b_q \end{bmatrix} \tag{8}$$

where K_d and K_q are the control gains. Here, the feedback linearizing control $\boldsymbol{u_0}$ is denoted by the baseline controller or the nominal control law. This is because the control design of $\boldsymbol{u_0}$ assumes exact knowledge of the parameters of the system including the disturbance $\boldsymbol{b}$. The tracking errors e_d and e_q are defined as follows

$$e_d = i_{dref} - i_d; \quad e_q = i_{qref} - i_q \tag{9}$$

i_{dref} and i_{qref} are the d-axis current reference and the q-axis current reference, respectively. The closed-loop dynamic equations can be obtained by substituting (8) in (1), leading to

$$\dot{e}_d + K_d e_d = 0; \quad \dot{e}_q + K_q e_q = 0 \tag{10}$$

In the case of a step input, the reference-to-output transfer function can be determined by substituting $\dot{i}_{dref} = 0$ and $\dot{i}_{qref} = 0$ in (10), yielding

$$\frac{I_d(s)}{I_{dref}(s)} = \frac{K_d}{s + K_d}; \quad \frac{I_q(s)}{I_{qref}(s)} = \frac{K_q}{s + K_q} \tag{11}$$

where $I_{d,q}$ is the Laplace transform of $i_{d,q}$. The above equation indicates that the current loop reduces to a first-order system with a time constant equal to $1/K_{d,q}$. Unfortunately, the target behavior, specified by (11), cannot be practically achieved as the implementation of the FBL requires the information about the disturbances $\boldsymbol{b}$. Such information can be obtained through the use of a disturbance observer; therefore, the controller (8) reduces to

$$\boldsymbol{u} = B^{-1} \begin{bmatrix} K_d e_d + \dot{i}_{dref} - f_d(\boldsymbol{x}) \\ K_q e_q + \dot{i}_{qref} - f_q(\boldsymbol{x}) \end{bmatrix} - \begin{bmatrix} \hat{b}_d \\ \hat{b}_q \end{bmatrix} \tag{12}$$

where $\hat{b}_d$ and $\hat{b}_q$ are the disturbance estimations. In the case of a step input, it is clear that the controller (12) is implemented as

$$\boldsymbol{u} = B^{-1} \begin{bmatrix} K_d e_d - f_d(\boldsymbol{x}) \\ K_q e_q - f_q(\boldsymbol{x}) \end{bmatrix} - \begin{bmatrix} \hat{b}_d \\ \hat{b}_q \end{bmatrix} \tag{13}$$

III. Design of the Disturbance Observer-Based Control

A. Disturbance Observer-Based Control (DOBC)

As in [26], an initial disturbance observer can be written as

$$\dot{\hat{\boldsymbol{b}}} = -l(\boldsymbol{x}) B\hat{\boldsymbol{b}} + l(\boldsymbol{x})\left(\dot{\boldsymbol{x}} - \boldsymbol{f}(\boldsymbol{x}) - B\boldsymbol{u}\right) \tag{14}$$

where $l(\boldsymbol{x})$ is a 2×2 real matrix that represents the observer gain. The matrix $l(\boldsymbol{x})$ can be expressed as

$$l\left(\boldsymbol{x}\right) = \frac{\partial \boldsymbol{p}\left(\boldsymbol{x}\right)}{\partial \boldsymbol{x}} \tag{15}$$

with $\boldsymbol{p}(\boldsymbol{x})$ is a vector function to be designed. In the presence of the saturation blocks, the DOBC (14) becomes

$$\dot{\hat{\boldsymbol{b}}} = -l\left(\boldsymbol{x}\right) B\hat{\boldsymbol{b}} + l\left(\boldsymbol{x}\right)\left(\dot{\boldsymbol{x}} - \boldsymbol{f}\left(\boldsymbol{x}\right) - B\boldsymbol{u_{sat}}\right) \tag{16}$$

where $\boldsymbol{u_{sat}}$ is the output of the saturation blocks, and it is computed as

$$\boldsymbol{u_{sat}} = sat\left(\boldsymbol{u}\right) = \begin{cases} u_{min}, & u < u_{min} \\ u, & u \in [u_{min}, u_{max}] \\ u_{max}, & u > u_{max} \end{cases} \tag{17}$$

combining (16) with (1) leads to

$$\dot{\hat{\boldsymbol{b}}} - \dot{\boldsymbol{b}} = -l\left(\boldsymbol{x}\right) B\left(\hat{\boldsymbol{b}} - \boldsymbol{b}\right) - \dot{\boldsymbol{b}} \tag{18}$$

Let $\boldsymbol{e_b}$ be the disturbance estimation error as $\boldsymbol{e_b} = \hat{\boldsymbol{b}} - \boldsymbol{b}$, then (18) reduces to

$$\dot{\boldsymbol{e}}_{\boldsymbol{b}} = -l\left(\boldsymbol{x}\right) B\boldsymbol{e_b} - \dot{\boldsymbol{b}} \tag{19}$$

As B is a constant diagonal matrix, the above dynamic equation can be made stable by choosing $l(\boldsymbol{x})$ to be a constant diagonal matrix as

$$l\left(\boldsymbol{x}\right) = l = \begin{bmatrix} l_d & 0 \\ 0 & l_q \end{bmatrix} \tag{20}$$

Invoking (15), $\boldsymbol{p}(\boldsymbol{x})$ can be chosen as

$$p\left(\boldsymbol{x}\right) = l\boldsymbol{x} = \begin{bmatrix} l_d i_d & l_q i_q \end{bmatrix}^{\mathsf{T}} \tag{21}$$

Combining (19)–(20) leads to

$$\dot{e}_{bd} = -\frac{l_d}{L_d} e_{bd} - \dot{b}_d; \qquad \dot{e}_{bq} = -\frac{l_d}{L_q} e_{bq} - \dot{b}_q \tag{22}$$

where $e_{bd} = \hat{b}_d - b_d$ and $e_{bq} = \hat{b}_q - b_q$ are the disturbance estimation errors, and

$$\boldsymbol{e_b} = \begin{bmatrix} e_{bd} & e_{bq} \end{bmatrix}^{\mathsf{T}} \tag{23}$$

From (22), it follows that the disturbance estimation error $\boldsymbol{e_b}$ is bounded for any bounded $\dot{\boldsymbol{b}}$ provided that the observer gain is chosen as $l_\eta > 0$, with $\eta = \{d, q\}$. The asymptotic stability of the origin $\boldsymbol{e_b} = 0$ is guaranteed under the condition

$$\lim_{t \to \infty} \dot{b}_\eta = 0; \quad \eta = \{d, q\} \tag{24}$$

The above condition is always satisfied for the system under study. This is because, at the steady-state regime, the PMSG usually operates under a constant set-point.

The real-time implementation of (14) requires the measurement of the time derivative of the state which is not always available. To address such a problem, the disturbance observer can be implemented as follows

$$\begin{cases} \dot{\hat{\boldsymbol{z}}} = -lB\left(\hat{\boldsymbol{z}} + \boldsymbol{p}(\boldsymbol{x})\right) - l\left(\boldsymbol{f}(\boldsymbol{x}) + B\boldsymbol{u_{sat}}\right) \\ \hat{\boldsymbol{b}} = \hat{\boldsymbol{z}} + \boldsymbol{p}(\boldsymbol{x}) \end{cases} \tag{25}$$

The block diagram for implementing the composite controller using the DOBC (25) is depicted in Fig. 2. As all states are measurable, i.e., $\boldsymbol{y} = \boldsymbol{x}$ and $\boldsymbol{p}(\boldsymbol{x}) = l\boldsymbol{x} = l\boldsymbol{y}$, the above disturbance observer can be viewed as a reduced-order high-gain observer [22]. Therefore, for sufficiently high observer gain, the composite controller can retain the nominal transient performance achieved under the feedback linearizing control, particularly when the control input does not saturate during transients [21]. In other words, the composite controller is able to produce the transient behavior, defined by (11), provided that l_η is high enough.

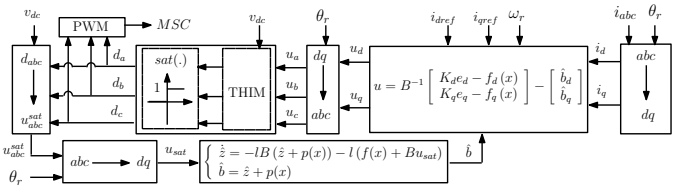

Fig. 2. Block diagram of the composite controller using the DOBC. Here, THIM denotes third harmonic injection method used for generating the modulating signals d_a, d_b, and d_c. The actual control u_{abc}^{sat} is approximated as $u_{abc}^{sat} = (d_{abc} - 0.5)\, v_{dc}$

B. PI-Disturbance Observer

The DOBC can be further simplified to make it more convenient for real time-implementation. To do so, note that the initial disturbance observer (16) can be rewritten as

$$\dot{\hat{\boldsymbol{b}}} = -lB\hat{\boldsymbol{b}} + l\left(\dot{\boldsymbol{x}} - \boldsymbol{f}\left(\boldsymbol{x}\right) - B\boldsymbol{u} + B\bar{\boldsymbol{u}}\right) \tag{26}$$

where

$$\bar{\boldsymbol{u}} = \boldsymbol{u} - \boldsymbol{u_{sat}} \tag{27}$$

Now, substituting (12) into (26) gives

$$\dot{\hat{\boldsymbol{b}}} = -lK\boldsymbol{e} - l\dot{\boldsymbol{e}} + lB\bar{\boldsymbol{u}} \tag{28}$$

where K is a 2×2 diagional matrix, representing the control gain, and $\boldsymbol{e}$ is the tracking error. That is

$$K = diag\{K_d, K_q\}; \quad \boldsymbol{e} = \begin{bmatrix} e_d & e_q \end{bmatrix}^{\mathsf{T}} \tag{29}$$

The PI disturbance observer can be obtained by integrating the above equation, yielding

$$\hat{\boldsymbol{b}} = -lK\int_0^t \boldsymbol{e}\left(\tau\right) d\tau - l\boldsymbol{e} + \bar{\boldsymbol{b}}(0) + \boldsymbol{u_a} \tag{30}$$

where

$$\bar{\boldsymbol{b}}(0) = l\boldsymbol{e}\left(0\right) + \hat{\boldsymbol{b}}\left(0\right); \qquad \boldsymbol{u_a} = lB\int_0^t \bar{\boldsymbol{u}}\left(\tau\right) d\tau \tag{31}$$

In the absence of information about the disturbance $\boldsymbol{b}$, the initial term $\hat{\boldsymbol{b}}(0)$ is set to be equal to zero in order to ease the real-time implementation of the composite controller. The term $\boldsymbol{u_a}$ is basically an anti-windup compensator that has the role of eliminating the undesired effect of the saturation block required to limit the modulating signal fed to the Pulse Width Modulation (PWM) technique. In the case of a filtered reference, the initial tracking error is equal to zero, i.e, $\boldsymbol{e}(0) = 0$, meaning that the PI-disturbance observer reduces to a PI controller plus an anti-windup scheme. In other words, for a smooth reference, the composite controller consisting

of the feedback controller (12) and the PI-DO (30)–(31) is able to achieve a good tracking performance under model uncertainty. In the case of a step input with a constant set-point, the PI-disturbance observer (30)–(31) can be considered as an exact representation of the disturbance observer (16). However, in the case of a step input with a variable set-point, the PI-disturbance observer (30)–(31) can no longer represent the transient performance of the disturbance observer (25). More specifically, in the case of a step input, the disturbance observer (28) can be rewritten as

$$\begin{aligned}\dot{\hat{\boldsymbol{b}}} &= -lK\boldsymbol{e} - l\dot{\boldsymbol{y}}_{ref} + l\dot{\boldsymbol{y}} + lB\bar{\boldsymbol{u}} \\ &= -lK\boldsymbol{e} + l\dot{\boldsymbol{y}} + lB\bar{\boldsymbol{u}}\end{aligned} \tag{32}$$

where $\boldsymbol{y_{ref}} = \begin{bmatrix} i_{dref} & i_{qref} \end{bmatrix}^{\intercal}$ is the reference and $\dot{\boldsymbol{y}}_{\boldsymbol{ref}} = 0$. Now, integrating (32) gives

$$\hat{\boldsymbol{b}} = -lK\int_0^t \boldsymbol{e}(\tau)\,d\tau + l\boldsymbol{y} - l\boldsymbol{y}(0) + \hat{\boldsymbol{b}}(0) + \boldsymbol{u_a} \tag{33}$$

which can be rewritten as

$$\hat{\boldsymbol{b}} = -lK\int_0^t \boldsymbol{e}(\tau)\,d\tau - l\boldsymbol{e} + \bar{\boldsymbol{b}} + \boldsymbol{u_a} \tag{34}$$

The term $\bar{\boldsymbol{b}}$ is expressed as

$$\bar{\boldsymbol{b}} = l\boldsymbol{y_{ref}} - l\boldsymbol{y}(0) + \hat{\boldsymbol{b}}(0) = l\boldsymbol{e}(0) + \hat{\boldsymbol{b}}(0) + \boldsymbol{\gamma} \tag{35}$$

where

$$\boldsymbol{\gamma} = l\boldsymbol{y_{ref}} - l\boldsymbol{y_{ref}}(0) \tag{36}$$

Invoking (31), it follows that

$$\bar{\boldsymbol{b}} = \bar{\boldsymbol{b}}(0) + \boldsymbol{\gamma} \tag{37}$$

The proposed PI-DO can be implemented using the block diagram shown in Fig. 3.

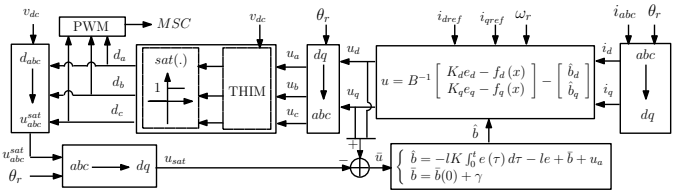

Fig. 3. Block diagram of the composite controller using the PI-DO. Here, THIM, $d_{\{a,b,c\}}$, and u_{abc}^{sat} are as defined in Fig. 2. Note that the PI-DO (30)–(31) corresponds to the case of $\gamma = 0$.

Clearly, the only difference between the disturbance observers (30)–(31) and (34)–(37) lies in the introduction of an additional term $\boldsymbol{\gamma}$ for the case of a step input. Specifically, the additional term $\boldsymbol{\gamma}$ represents the reference jump which can also be viewed as a transient disturbance. Therefore, neglecting this term for the case of a step input will make the disturbance observer deal with the sudden step change in the reference as a disturbance input. Thereby, the disturbance observer will eventually produce inaccurate transient estimation in attempt to compensate for the step change in the reference. This explains why, the disturbance observer (30)–(31) cannot produce the transient behavior of the DOBC (25) particularly after a sudden change in the set-point. However, the introduction of $\boldsymbol{\gamma}$ allows canceling the effect of the reference jump on the transient performance of the disturbance observer, making the output of the observer insensible to the step change in the reference.

IV. Closed-loop Stability and PI Current Controller

A. Closed-Loop Stability

Substituting the controller (12) into the system model (1) gives

$$\dot{e}_d = -K_d e_d + \frac{1}{L_d}e_{bd}; \qquad \dot{e}_q = -K_q e_q + \frac{1}{L_q}e_{bq} \tag{38}$$

From (22) and (38), it can be verified that

$$\begin{bmatrix} \dot{\boldsymbol{e}} \\ \dot{\boldsymbol{e}}_b \end{bmatrix} = \begin{bmatrix} -K & B \\ 0_{2\times 2} & -Bl \end{bmatrix}\begin{bmatrix} \boldsymbol{e} \\ \boldsymbol{e_b} \end{bmatrix} - \begin{bmatrix} 0_{2\times 1} \\ \dot{\boldsymbol{b}} \end{bmatrix} \tag{39}$$

The matrix Bl is given by

$$Bl = diag\{\frac{l_d}{L_d}, \frac{l_q}{L_q}\} \tag{40}$$

Considering (29) and (40), the eigenvalues of the closed-loop system (39) are $\sigma_{1:4} = -\{K_d, K_q, l_d/L_d, l_q/L_q\}$. As all the eigenvalues are negative, then, under $\dot{\boldsymbol{b}} = 0$, the closed-loop system (39) has a globally exponentially stable equilibrium point at $\boldsymbol{e} = 0$ and $\boldsymbol{e_b} = 0$. Thereby, following the Lemma 4.6 in [25], the closed-loop system is input-to-state stable with respect to the disturbance input $\dot{\boldsymbol{b}}$. In other words, the errors $\boldsymbol{e}$ and $\boldsymbol{e_b}$ are bounded for any bounded $\dot{\boldsymbol{b}}$, and the bounds on $\boldsymbol{e}$ and $\boldsymbol{e_b}$ are proportional to $\dot{\boldsymbol{b}}$. This implies that the steady-state error converges to zero, provided that $\lim_{t\to\infty} \dot{\boldsymbol{b}} = 0$.

B. Decoupled PI Current controller

The decoupled PI current controller, under a step input, can be obtained by substituting (34)–(37) into (13), yielding

$$u_d = P_d e_d + N_d\int_0^t e_d(\tau)\,d\tau + D_d - u_{ad} - \bar{b}_d \tag{41}$$

and

$$u_q = P_q e_q + N_q\int_0^t e_q(\tau)\,d\tau + D_q - u_{aq} - \bar{b}_q \tag{42}$$

The gains of the PI controller are determined as

$$P_{d,q} = L_{d,q}K_{d,q} + l_{d,q}; \qquad N_{d,q} = l_{d,q}K_{d,q} \tag{43}$$

The components of the anti-windup compensator $\boldsymbol{u_a}$ are given by

$$u_{ad} = \frac{l_d}{L_d}\int_0^t \bar{u}_d(\tau)\,d\tau; \quad u_{aq} = \frac{l_q}{L_q}\int_0^t \bar{u}_q(\tau)\,d\tau \tag{44}$$

The decoupling terms $D_d(\boldsymbol{x})$ and $D_q(\boldsymbol{x})$ are expressed as

$$D_d = Ri_d - L_q p\omega_r i_q; \quad D_q = Ri_q + L_d p\omega_r i_d + \phi_v p\omega_r \tag{45}$$

From (31) and (36)–(37), it follows that

$$\begin{cases} \bar{b}_d = le_d(0) + l_d(i_{dref} - i_{dref}(0)) \\ \bar{b}_q = le_q(0) + l_q(i_{qref} - i_{qref}(0)) \end{cases} \tag{46}$$

The resulting PI current controller can be practically implemented using the block diagram shown in Fig. 4.

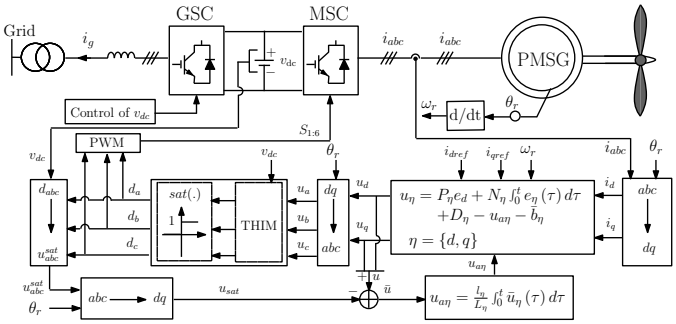

Fig. 4. Block diagram of the proposed PI current controller for the PMSG-based WECS. For the system under study, the current is always null at $t = 0$, i.e., $i_\eta(0) = 0$. Therefore, from (46), $e_\eta(0) = i_{\eta ref}(0) \rightarrow \bar{b}_\eta = l i_{\eta ref}$.

Remark 1: The term $\boldsymbol{\gamma}$ in (36) is derived based on the assumption that the current reference is represented by step commands, i.e, $\dot{\boldsymbol{y}}_{\boldsymbol{ref}} = 0$. However, in the case of a smooth reference, the term $\boldsymbol{\gamma}$ will not appear in (37) which implies that $\boldsymbol{\gamma}$ will be removed from the PI current controller. In such a case, the tracking problem can be solved by using the composite controller, consisting of the control law (12) and the PI-DO (30)–(31), with $\boldsymbol{e}(0) = 0$. This makes the time derivative of the reference arise naturally in the resulting PI controller. More specifically, in the case of a filtered reference, the terms $\bar{b}_d$ and $\bar{b}_q$ in (41)–(42) are replaced by $-L_d\dot{i}_{dref}$ and $-L_q\dot{i}_{qref}$, respectively. In other words, for a smooth reference, the term $\bar{b}_\eta$ in Fig. 4 will be replaced by $-L_\eta\dot{i}_{\eta ref}$.
Remark 2: The use of the time derivative of the reference allows the resulting PI controller to achieve a good tracking performance if the control objective is to track a smooth reference. However, the time derivative of the reference may magnify the measurement noises if the current reference is provided by an outer block that uses the actual measurement to determine the current command. Examples of these blocks include MPPT algorithm and outer voltage loop to regulate the DC-link voltage in cascade control scheme. The proposed PI controller (41)–(42) can also achieve a good track of a smooth reference command even though it is designed for step reference commands. Therefore, the proposed decoupled PI current controller can be extended to the case of cascade control schemes with a view to prevent magnification of the measurement noises.

V. Experimental Results

A. Laboratory Setup

The laboratory setup was composed of a 22-pole, 5 kW PMSG that fed a 5 kW, 3ϕ six-pulse IGBT inverter. The output of the inverter was connected to the input terminals of a 5 kW, 3ϕ, six-pulse IGBT-based controlled rectifier via a DC-Link capacitor as shown in the Fig. 5. The output terminals of the IGBT-based controlled rectifier were connected to the secondary side of a 16 kVA, 3ϕ, 50 Hz auto-transformer through an L filter. Furthermore, a 22-pole, 6 kW PMSM was used as wind turbine emulator to drive the PMSG at the desired speed. The stator windings of the PMSM were supplied through a 5 kW, 3ϕ industrial drive that was fed directly from the secondary of the auto-transformer. Real-implementation of the proposed controller was facilitated by a dSPACE MicroLabBox (DS1102). The rotor position θ_r and the 3ϕ stator currents were measured and fed to DS1102 board. The parameters of the PMSG are given in the appendix.

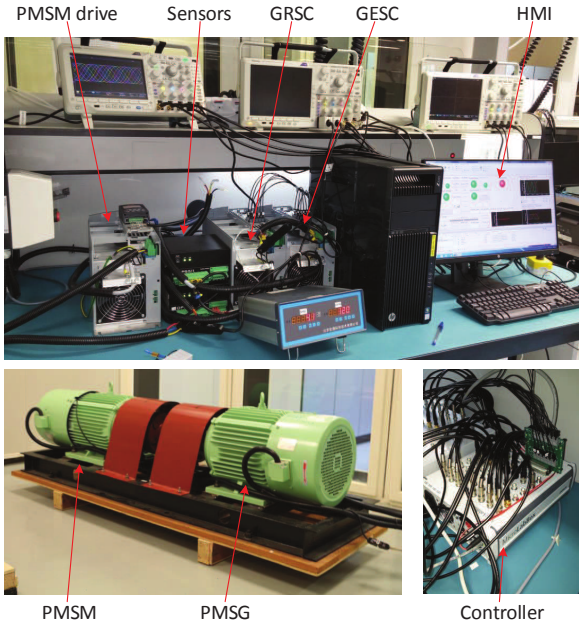

Fig. 5. Laboratory setup for PMSG-based wind turbine.

B. Experimental Conditions

Following (11), the controller gains K_d and K_q can be selected based on the performance specification of the settling time t_s, defined as $t_s = 4K_{d,q}^{-1}$. Thus, selecting $K_{d,q} = 1000$ implies that the dq-axis current takes about 4 ms to reach its reference with zero steady-state error. The observer gains l_d and l_q should be selected as large as feasible to recover the nominal transient performance of the state feedback controller despite the presence of modeling errors. In real-time implementation, high observer gain may amplify the measurement noises, leading to poor steady-state performances. Therefore, the observer gains should be carefully selected to avoid the magnification of the measurement noises. In this work, l_d and l_q are set to 30 and 40, respectively. The control scheme of the GSC consists of two loops; an inner-loop for controlling the active and reactive powers and an outer-loop for adjusting the DC-link voltage to 370 V. The controller of the GSC is implemented as presented in [27]. The rotor speed of the PMSG is fixed to $\Omega_r = -200$ rpm, with $\omega_r = (\pi/30)\Omega_r$. The negative sign of the rotor speed is dictated by the configuration of the laboratory setup. Therefore, the q-axis current reference should be positive to make the machine operate as a generator. The sampling frequency of the controller is set to 10 kHz. Both GSC and MSC are operated at a switching frequency of 10 kHz. Observation of the block diagrams, depicted in Figs. 2, 3, and 4, shows that the modulating signals d_a, d_b,

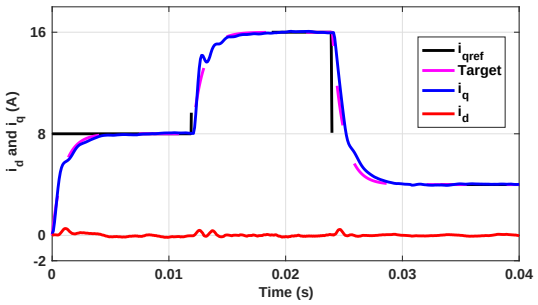

(a) dq axis current response with the consideration of γ

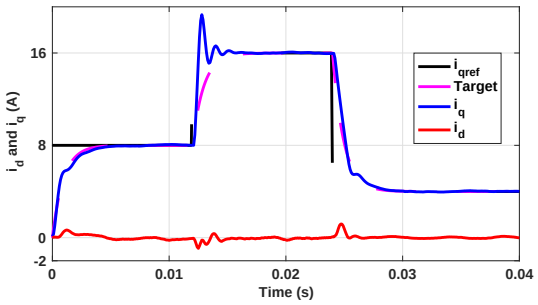

(b) dq axis current response without the consideration of γ, i.e., $\gamma = 0$

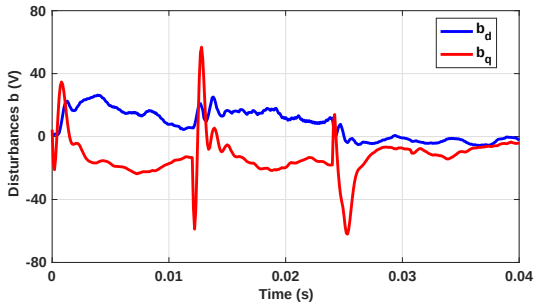

(c) Disturbance estimation with the consideration of γ

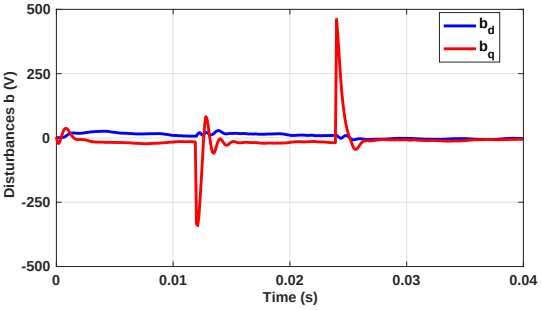

(d) Disturbance estimation without the consideration of γ, i.e., $\gamma = 0$

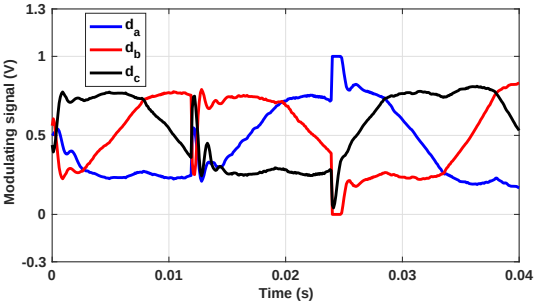

(e) Modulating signals with the consideration of γ

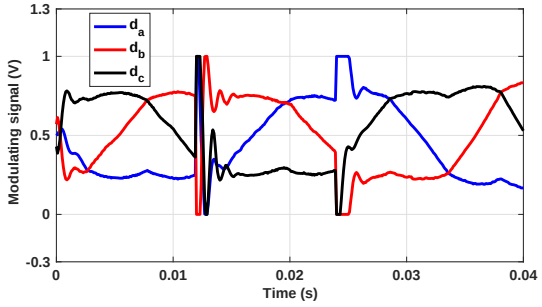

(f) Modulating signals without the consideration of γ, i.e., $\gamma = 0$

Fig. 6. System's response under the composite controller consisting of the feedback controller (13) and the PI-DO (34)–(37). The controller was tested experimentally using the block diagram of Fig. 3. Specifically, the PI-DO (34)–(37) was evaluated with and without the consideration of the reference jump γ.

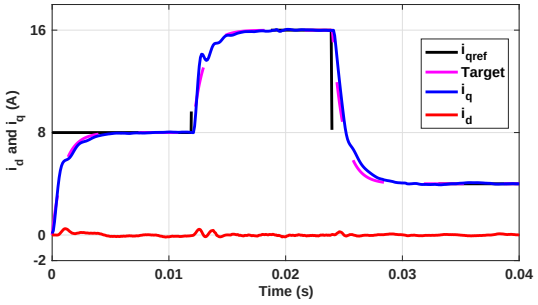

(a) dq axis current response.

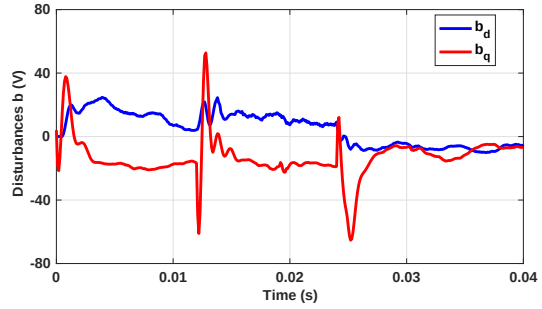

(b) Disturbance estimation with the DOBC (25).

Fig. 7. System's response under the composite controller consisting of the feedback controller (13) and the DOBC (25). The controller was tested experimentally using the block diagram depicted in Fig. 2.

and d_c are generated using the third harmonic injection PWM to increase the voltage capability of the inverter. The limitation of the modulating signal is realized through the use of saturation blocks to avoid over-modulation during transients.

C. Performance Evaluation of the PI-DO and the DOBC Under Nominal Parameters

In this test, the PMSG was controlled to generate a variable power at a fixed rotor speed of $\Omega_r = -200$ rpm. Toward

this end, the d-axis current reference was set to 0 while the q-axis current reference was initiated at 8 A, steeped up to 16 A at $t = 12$ ms, and steeped down to 4 A at $t = 24$ ms. From the parameters of the machine, the q-axis current reference corresponded to step changes in the delivered power as $P_g : 0 \rightarrow 1.67 \rightarrow 3.35 \rightarrow 0.83$ kW. The controller was implemented using the nominal parameters that were identified in the laboratory. The results in Fig. 6(a)–(d) show that the step changes in the current reference clearly affect the output of the PI-DO in both cases, i.e., with and without the reference jump $\boldsymbol{\gamma}$. However, it is clear that the magnitude of the disturbance estimation, during transients, is relatively very large when the reference jump is not included in the PI-DO. This is because the PI-DO treats the current reference jump as a transient disturbance that should be estimated. Thus, introducing the reference jump in the PI-DO allows to attenuate the effect of the sudden jump in the reference and to improve the accuracy of the PI-DO. As could be seen in Fig. 6(c), the transient behavior of the proposed PI-DO is still sensible to the step changes in the current command even though no disturbance is applied to the system. From the theoretical standpoint, the output of the proposed PI-DO should remain unchanged after a sudden jump in the reference if no disturbance is applied to the system. However, in practice, transient disturbances are inevitable at the time of application of a step change in the reference due to many factors, including time-delay, model parameter uncertainties associated with the identification process, and the transient variation of the rotor speed caused by the abrupt increase/decrease in the power command. This explains why the proposed PI-DO produces such a transient behavior following the step changes in the current reference. Fig. 6(a) shows that the q-axis current closely tracks the 'Target' specified by the state-feedback control law under nominal conditions, particularly when the control does not saturate. This evidences the ability of the proposed PI-DO to retain the nominal transient performance specified under feedback linearizing control. During control saturation, Figs. 6(a) and 6(e) show that the anti-windup scheme performed very well, as no overshoot was observed despite the saturation of the controller in response to the step decrease in the current reference.

Another test was conducted to show the equivalency between the DOBC (25) and its simplified version (34)–(37). The experimental results in Figs. 6(c) and 7(b) demonstrate the ability of the proposed PI-DO to accurately represent the DOBC in both transient and steady-state regimes, which confirms the efficacy of the design methodology.

D. Comparison Between the Proposed PI Controller and a Conventional PI Controller Under Nominal parameters

In this test, a conventional PI current controller was implemented as presented in [17] together with an anti-windup method. The d-axis current reference was kept equal zero, and the q-axis current reference was changed as $i_{qref} : 0 \rightarrow 4 \rightarrow 8 \rightarrow 16$ A. Following [17], the coefficients P_η and N_η of the conventional PI controller were determined as $L_\eta \omega_{cc}$ and $R\omega_{cc}$, respectively. ω_{cc} is the bandwidth of the closed-loop system, and it should be selected to correspond to the desired settling time. Specifically, by considering the effective back-EMF, the reference-to-output transfer function reduces to a first-order system whose expression is given by (49) in the Appendix. As in [17], the gain of the anti-windup scheme was selected as R/L_η. To perform a fair comparison, both PI controllers should be tuned to have the same closed-loop transfer function, meaning that ω_{cc} should be selected equal to the control gain $K_{d,q} = 1000$. In this test, the conventional PI controller was tested using three values of ω_{cc}; 1000, 1200 and 3000 rad/s. Fig. 8 shows the current response under ω_{cc} equal to 1200 and 3000 rad/s, where 'Target' represents the response of the nominal closed-loop system under the conventional PI controller. As shown in Fig. 8(a), when tuned with $\omega_{cc} = 1200$, the conventional PI controller is able to provide an acceptable transient behavior, but the closed-loop settling time is much larger than the nominal one which is about $4\omega_{cc}^{-1}$. The results with $\omega_{cc} = 1000$ were not plotted, because it is clear that it results in larger settling time. Fig. 8(b) shows that increasing ω_{cc} reduces the closed-loop settling time, but this particular design results in serious degradation of the transient response by causing a large overshoot. In conclusion, compared with the proposed PI controller, the conventional PI current controller cannot retain the transient response of the nominal closed-loop system governed by (49).

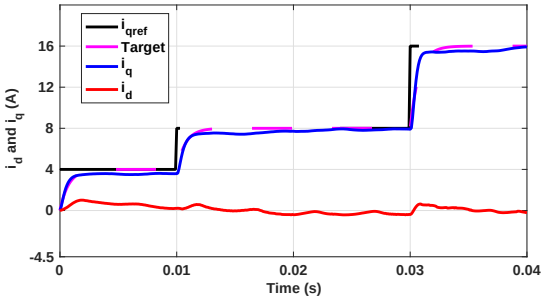

(a) dq axis current response under the existing PI controller [17], with $\omega_{cc} = 1200$.

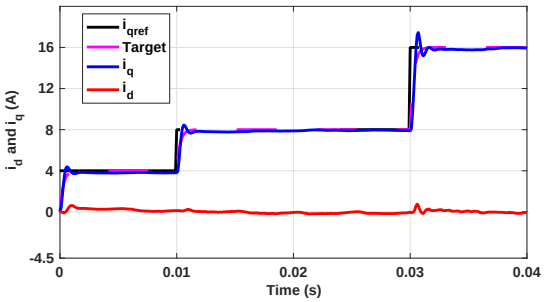

(b) dq axis current response under the existing PI controller [17], with $\omega_{cc} = 3000$.

Fig. 8. System's response under a conventional PI current controller [17].

E. Performance Evaluation of the Proposed PI-DO Under Model Uncertainty

This test aimed to demonstrate the ability of the proposed PI-DO to guarantee the nominal transient performance in

response to step changes in the current command, particularly when the model parameters were incorrectly set in the controller. Toward this end, the values of R, L_d, and ϕ_v were chosen equal to 50%, 50%, and 80% of their nominal values, respectively. Here, the measured currents, the duty-cycle, and the disturbance estimation were displayed using a Tektronix digital phosphor oscilloscope. Fig. 9(a)–(b) confirmed the ability of the proposed controller to reshape the nominal transient performance in spite of the modeling errors. Fig. 9(b) shows how the disturbance estimation behaves to cancel out the model parameter uncertainty, while Fig. 9(c) gives the modulating signals computed with the use of the third harmonic injection method.

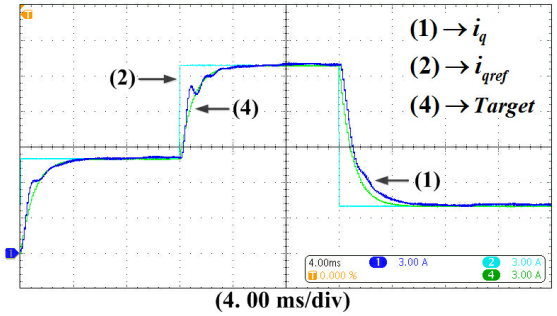

(a) q axis current response

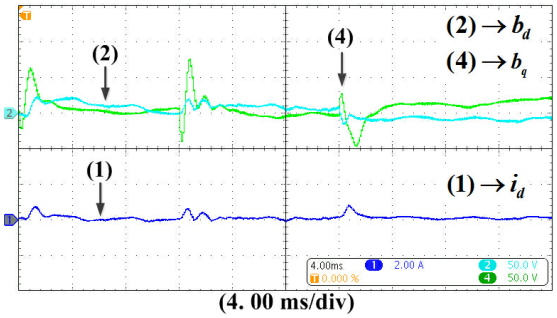

(b) Disturbance estimation and d-axis current

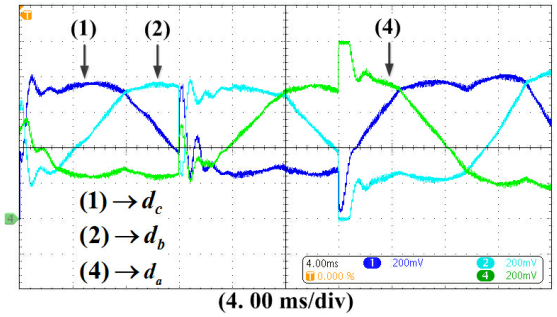

(c) Modulating signals d_{abc}

Fig. 9. Performance evaluation of the proposed PI-DO under model uncertainty.

F. Performance Evaluation under Wind Speed Variations: MPPT Operation

The objective of this experiment was to investigate the effectiveness of the proposed PI curent controller (41)–(46) under variable wind speed conditions. In particular, this test was performed under rotor speed variations to emulate wind speed variation. The resulting PI current controller was experimentally tested using the block diagram shown in Fig. 4. For a given wind speed ω_s (m/s), the maximum power can be extracted from the wind by regulating the rotor speed at $\omega_{rref} = nw_s\lambda_{opt}/R_b$ [28], where, n and R_b are the gear ratio and the rotor plane radius (m), respectively. λ is the tip speed ratio (TSR) of the blade, and its optimal value λ_{opt} is selected to correspond to the maximum value C_{pmax} of the power coefficient curve C_p of the emulated wind turbine [8]. In this experiment, a PMSM drive, representing the wind turbine emulator, is used to regulate the rotor speed of the PMSG at a desired level. Therefore, no outer loop is required to regulate the rotor speed of the PMSG. Nonetheless, the q-axis current reference i_{qref} can be calculated based on the optimal torque T_{gopt} with the aim of achieving MPPT operation. Following [8], the optimal torque can be expressed as $T_{gopt} = K_{opt}\omega^2_{rref}$, where the constant K_{opt} depends on the characteristic of the wind turbine and is given in the Appendix A. The optimal reference for the q-axis current can be computed by substituting the expression of the optimal torque T_{gopt} into (6) as presented in the Appendix A.

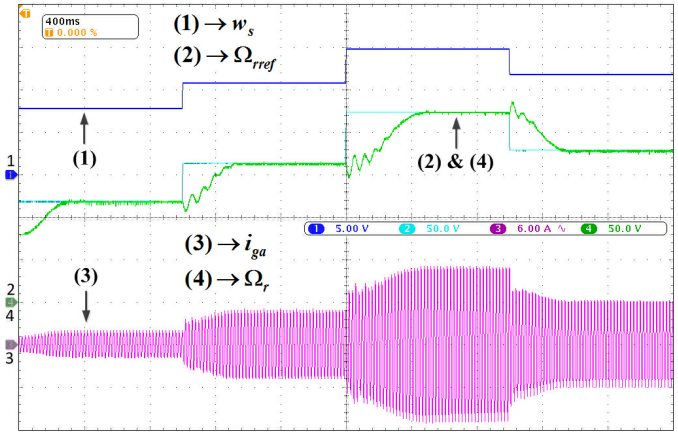

(a) Wind speed profile and system's response under an MPPT algorithm, with i_{ga} is the grid current and $\Omega_{rref} = (30/\pi)\omega_{rref}$.

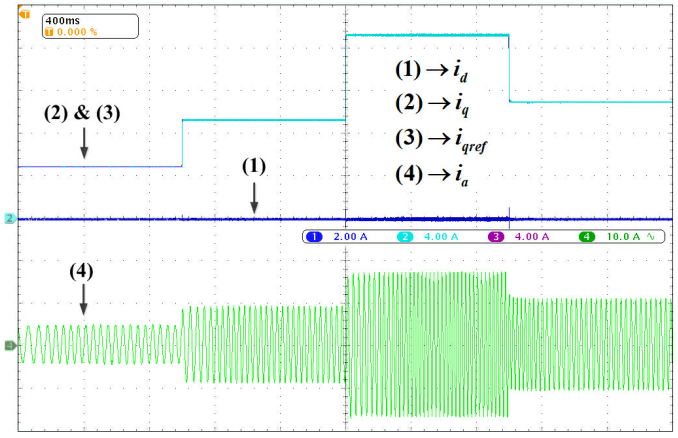

(b) System's response under MPPT algorithm, with i_a is the phase current.

Fig. 10. Experimental results: Performance testing of the proposed PI current controller under MPPT algorithm, with i_d (2 A/div), i_q (4 A/div), i_a (10 A/div), w_s (5 [m/s]/div), i_{ga} (6 A/div), Ω_r (50 [rpm/min]/div), and time (400 ms/div)

Fig. 10 shows the current response to step changes in wind speed. The profile of the wind speed is realized as $w_s : 8 \rightarrow 11 \rightarrow 15 \rightarrow 12$ m/s, where the duration of each step is set to 1 s. As can be seen in Fig. 10(a), the rotor speed of the PMSG is well controlled, and the transient tracking error between the rotor speed and its set-point can be explained by the limited dynamics of the PMSM drive. The experimental results, shown in Fig. 10(b), demonstrate the ability of the proposed PI current controller to acheive good transient and steady-state performances. Fig. 10 also presents the waveforms of the grid current and the current flowing through the stator winding of the PMSG.

VI. Conclusion

This paper has presented a novel design of decoupled PI controller to enhance the transient performance for the current control of PMSG-based wind turbine. The proposed controller technique was established by combining a DOBC with feedback linearizing control law. It turns out that the composite controller has a decoupled PI-like structure plus two additional parts. The first part is basically an anti-windup compensator, while the second part uses the reference jump information to cancels out the effect of the sudden step changes in the power demand on the transient response. This modification of the decoupled PI controller permits to guarantee zero steady-state error without sacrificing the nominal transient performance specified by the state feedback controller. This salient feature cannot be achieved under the existing decoupled PI controller, particularly when the model parameters are not accurate. Experimental tests have been performed, and the results support the use of the reference jump information to improve the transient performance under the decoupled PI controller. Therefore, the proposed approach provides practitioners with an alternate method in designing a robust decoupled PI current controller for PMSG-based wind energy conversion system.

Appendix A
Derivation of the q-axis current reference under MPPT Algorithm

Following [8], [28], the constant K_{opt} is given by

$$K_{opt} = \frac{\rho \pi R_b^2}{2} C_{p\max} \left(\frac{R_b}{n \lambda_{opt}} \right)^3 \tag{47}$$

where, ρ is the air density (kg/m^3). The optimal reference for the q-axis current can be determined by setting $i_d = 0$ into (6), yielding

$$i_{qref} = \frac{2}{3p\phi_v} K_{opt} \omega_{rref}^2 \tag{48}$$

Appendix B
Parameters of the system

The Parameters values of the 5 kW PMSM are $R = 0.84\ \Omega$, $L_d = 12.6$ mH, $L_q = 21.8$ mH, $\phi_v = 0.609$ Wb, $J = 1.6554$ Kgm^2, $B = 0.0594$ Nm.s/rad, and $p = 11$, $v_{dc} = 370$ V, where J is the moment of inertia and B is the coefficient of friction.

The power coefficient curve C_p is chosen as presented in [8], with $\lambda_{opt} = 6.36$ and $C_{pmax} = 0.4382$. The numerical values of R_b and n are set to 1.2 m and 1/3.38, respectively.

Appendix C
PI current controller

The reference-to-output transfer function under the conventional PI current controller is defined as

$$\frac{I_\eta(s)}{I_{\eta ref}(s)} = \frac{\omega_{cc}}{s + \omega_{cc}}; \quad \eta = \{d, q\} \tag{49}$$

References

[1] N. A. Orlando, M. Liserre, R. A. Mastromauro, and A. Dell'Aquila, "A survey of control issues in PMSG-based small wind-turbine systems," *IEEE Trans. Ind. Inform.*, vol. 9, no. 3, pp. 1211–1221, Aug 2013.

[2] Y. Wang, J. Meng, X. Zhang, and L. Xu, "Control of PMSG-based wind turbines for system inertial response and power oscillation damping," *IEEE Trans. on Sustainable Energy*, vol. 6, no. 2, pp. 565–574, April 2015.

[3] S. Benelghali, M. E. H. Benbouzid, J. F. Charpentier, T. Ahmed-Ali, and I. Munteanu, "Experimental validation of a marine current turbine simulator: Application to a permanent magnet synchronous generator-based system second-order sliding mode control," *IEEE Trans. Ind. Electron*, vol. 58, no. 1, pp. 118–126, Jan 2011.

[4] C. Wei, Z. Zhang, W. Qiao, and L. Qu, "An adaptive network-based reinforcement learning method for MPPT control of PMSG wind energy conversion systems," *IEEE Trans. Power Electron.*, vol. 31, no. 11, pp. 7837–7848, Nov 2016.

[5] H. M. Yassin, H. H. Hanafy, and M. M. Hallouda, "Enhancement low-voltage ride through capability of permanent magnet synchronous generator-based wind turbines using interval type-2 fuzzy control," *IET Renew. Power Gen.*, vol. 10, no. 3, pp. 339–348, 2016.

[6] L. Trilla, F. D. Bianchi, and O. Gomis-Bellmunt, "Linear parameter-varying control of permanent magnet synchronous generators for wind power systems," *IET Power Electron.*, vol. 7, no. 3, pp. 692–704, March 2014.

[7] F. Valenciaga and R. D. Fernandez, "Multiple-input-multiple-output high-order sliding mode control for a permanent magnet synchronous generator wind-based system with grid support capabilities," *IET Renew. Power Gen.*, vol. 9, no. 8, pp. 925–934, 2015.

[8] S. M. Mozayan, M. Saad, H. Vahedi, H. Fortin-Blanchette, and M. Soltani, "Sliding mode control of PMSG wind turbine based on enhanced exponential reaching law," *IEEE Trans. Ind.Electron.*, vol. 63, no. 10, pp. 6148–6159, Oct 2016.

[9] Z. Zhang, Y. Zhao, W. Qiao, and L. Qu, "A discrete-time direct torque control for direct-drive PMSG-based wind energy conversion systems," *IEEE Trans. Ind. Appl.*, vol. 51, no. 4, pp. 3504–3514, July 2015.

[10] A. Rajaei, M. Mohamadian, and A. Y. Varjani, "Vienna-rectifier-based direct torque control of PMSG for wind energy application," *IEEE Trans. Ind. Electron.*, vol. 60, no. 7, pp. 2919–2929, July 2013.

[11] A. Calle-Prado, S. Alepuz, J. Bordonau, P. Cortes, and J. Rodriguez, "Predictive control of a back-to-back NPC converter-based wind power system," *IEEE Trans. Ind. Electron.*, vol. 63, no. 7, pp. 4615–4627, July 2016.

[12] J. S. Lee and K. B. Lee, "Predictive control of vienna rectifiers for PMSG systems," *IEEE Trans. Ind. Electron.*, vol. 64, no. 4, pp. 2580 – 2591, Apl 2017.

[13] Z. Zhang, H. Fang, F. Gao, J. Rodríguez, and R. Kennel, "Multiple-vector model predictive power control for grid-tied wind turbine system with enhanced steady-state control performance," *IEEE Trans. Ind. Electron.*, vol. 64, no. 8, pp. 6287–6298, Aug 2017.

[14] S. Kouro, P. Cortes, R. Vargas, U. Ammann, and J. Rodriguez, "Model predictive control–a simple and powerful method to control power converters," *IEEE Trans. Ind. Electron.*, vol. 56, no. 6, pp. 1826–1838, June 2009.

[15] L. Xu, D. Zhi, and B. W. Williams, "Predictive current control of doubly fed induction generators," *IEEE Trans. Ind. Electron.*, vol. 56, no. 10, pp. 4143–4153, Oct 2009.

[16] S. Li, T. A. Haskew, R. P. Swatloski, and W. Gathings, "Optimal and direct-current vector control of direct-driven PMSG wind turbines," *IEEE Trans. Power Electron.*, vol. 27, no. 5, pp. 2325–2337, May 2012.

[17] Y. C. Kwon, S. Kim, and S. K. Sul, "Voltage feedback current control scheme for improved transient performance of permanent magnet synchronous machine drives," *IEEE. Trans. Ind. Electron.*, vol. 59, no. 9, pp. 3373–3382, Sept 2012.

[18] R. Cárdenas, E. Espina, J. Clare, and P. Wheeler, "Self-tuning resonant control of a seven-leg back-to-back converter for interfacing variable-speed generators to four-wire loads," *IEEE Trans. Ind. Electron.*, vol. 62, no. 7, pp. 4618–4629, July 2015.

[19] W.-J. Cao and J.-X. Xu, "Nonlinear integral-type sliding surface for both matched and unmatched uncertain systems," *IEEE Trans. Autom. Control*, vol. 49, no. 8, pp. 1355–1360, Aug 2004.

[20] M. Rubagotti, A. Estrada, F. Castaños, A. Ferrara, and L. Fridman, "Integral sliding mode control for nonlinear systems with matched and unmatched perturbations," *IEEE Trans. Autom. Control*, vol. 56, no. 11, pp. 2699–2704, Nov 2011.

[21] L. B. Freidovich and H. K. Khalil, "Performance recovery of feedback-linearization-based designs," *IEEE Trans. Autom. Control*, vol. 53, no. 10, pp. 2324–2334, Nov 2008.

[22] A. N. Atassi and H. K. Khalil, "A separation principle for the stabilization of a class of nonlinear systems," *IEEE Trans. Autom. Control*, vol. 44, no. 9, pp. 1672–1687, Sep 1999.

[23] W. Qiao, L. Qu, and R. G. Harley, "Control of IPM synchronous generator for maximum wind power generation considering magnetic saturation," *IEEE Trans. Ind. Appl.*, vol. 45, no. 3, pp. 1095–1105, May 2009.

[24] K. H. Kim, Y. C. Jeung, D. C. Lee, and H. G. Kim, "LVRT scheme of PMSG wind power systems based on feedback linearization," *IEEE Trans. Power Electron.*, vol. 27, no. 5, pp. 2376–2384, May 2012.

[25] H. K. Khalil, *Nonlinear systems*. Prentice hall Upper Saddle River, 2002, vol. 3.

[26] W.-H. Chen, D. J. Ballance, P. J. Gawthrop, J. J. Gribble, and J. O'Reilly, "Nonlinear PID predictive controller," *IEE Proc. Control Theory Appl.*, vol. 146, no. 6, pp. 603–611, 1999.

[27] R. Errouissi, A. Al-Durra, and S. M. Muyeen, "Design and implementation of a nonlinear PI predictive controller for a grid-tied photovoltaic inverter," *IEEE Trans. Ind. Electron.*, vol. 64, no. 2, pp. 1241–1250, 2016.

[28] S. A. Saleh and R. Ahshan, "Resolution-level-controlled WM inverter for PMG-based wind energy conversion system," *IEEE Trans. Ind. Appl.*, vol. 48, no. 2, pp. 750–763, March 2012.